Optimal Data Fusion for Pedestrian Navigation based on UWB and MEMS

V. Renaudin, B. Merminod
Ecole Polytechnique Fédérale de Lausanne
Switzerland

M. Kasser
Ecole Nationale des Sciences Géographiques
France

***Abstract* – Indoor pedestrian navigation is probably a very challenging research area. In this context, an optimal data fusion filter that hybridises a large set of observations: angles of arrival (AOA), time differences of arrival (TDOA), accelerations, angular velocities and magnetic field measurements is presented. The coupling of UWB and MEMS data relies on an Extended Kalman Filter complemented with specific procedures. Geometry based algorithms and a RANSAC paradigm that mitigates the Non Line Of Sight (NLOS) UWB propagation are detailed. The benefit of the solution is evaluated and compared with the pure inertial positioning system.**

I. Introduction

Outdoor positioning has been well explored and standardized whereas indoor positioning remains a recent research area that generates a multitude of new technical designs and algorithms. Table 1 compares some of the existing positioning systems. Localization and tracking technologies inside buildings are of great interest in many application fields, such as logistics, emergency services or personal navigation. This last domain is probably amongst the most challenging ones, due to the stochastic behaviour of human motion, and to the performances requested in terms of reliability and accuracy. A first level of requirement is pursued in the design of these technologies, since localization of emergency calls has become mandatory in many countries [1, 2]. Inside buildings, personal tracking systems address even higher requirements with one metre target accuracy.

The dominant systems can be divided into two main categories. The first category is the "network based local positioning systems" using sensor networks, mainly attached to the infrastructure of the building. Typical network based systems use some kind of signal to infer the distances between fixed elements, called the base stations (BS) and the mobile (M) that is to be located. Systems based on Bluetooth, ultra-wideband (UWB), IEEE 802.11b wireless fidelity or radio frequency identification belong to this category. They provide accurate positioning but fail when the signals are blocked [3]. The second category estimates the current location from a previously determined position using low cost inertial embedded sensors, such as Micro Electro Mechanical Sensors (MEMS). Dead reckoning methods and to a certain extent, assisted GPS (AGPS) belong to this category.

TABLE 1
Comparison of Indoor Positioning Systems [4]

Techno-logy	Process	Accuracy	Advantages	Limits
Network based local systems				
Blue-tooth RFID	Cell identity	Relative to the cell size	Simple and compatible with existing handset	Number and size of the cells
WiFi	AOA	up to 100 m	2 BS provide a position	Multipath, range to the BS, antenna quality
	TOA	1-50 m	High accuracy	Multipath, clock offset between M and BSs
	TDOA	1-50 m	High accuracy	Multipath
	RSS	Propagation models ~10m, Fingerprin-ting 1-5 m	High accuracy, compatible with existing hardware	Creation of RSS database / propagation models
UWB	AOA	Few decimetres	2 BS provide a position	Range to BS, antenna quality
	TDOA	Few decimetres	High accuracy	Low emission power, high BS density
Independent positioning systems				
AGPS	Network assisted ranging	Up to 5 m	Improved Time to first fix and signal tracking sensitivity	Multipath, not working in deep indoor
MEMS	Dead Reckoning	5% of travelled distance	Autonomous systems, position always available	Drifts affect the accuracy

Unfortunately, the performances of these "independent positioning systems" are affected by large errors (bias and noise) [5] typical of these sensors. In fact standalone solutions drift rapidly with time. Both categories present complementary advantages.

As UWB and MEMS are two of the most promising technologies in each category, this paper concentrates on indoor personal navigation algorithms that hybridise a large set of observed parameters: angles of arrival (AOA), time

1-4244-1537-3/08/$25.00 ©2008 IEEE

differences of arrival (TDOA), accelerations, angular velocities and magnetic field 3D measurements.

Section 2 presents several geometrical algorithms that process UWB signals. MEMS data are used to determine the biomechanical information describing the walking features, as described in section 3. An Extended Kalman Filter has been optimised for the fusion of the observations and complemented with a Random Sample Consensus procedure that mitigates the Non Line of Sight UWB propagation. This new method is detailed in section 4.

The proposed algorithms consider the limitations due to the human body absorption of radio signals, the limited and often non-redundant UWB observations and the physical constraints of the human motion. The results of experimental tests are presented in section 5, so as to evaluate the benefits of the solution and to compare the performances with the pure inertial location technique.

II. GEOMETRY BASED PROCESSING OF RADIO SIGNAL METRICS

In this section, the 3D mobile location estimation based on geometric processing of UWB metrics is depicted in details. First, the mathematical modelling of the signals metrics, that is the AOA and the TDOA, are formulated. Then the 3D geometry based mobile location estimation algorithms are presented for three different cases: intersection of two AOA, intersection of one AOA and one TDOA, intersection of two TDOA.

A. Modelling of angles of arrival

In the base station reference frame (BSRF), the horizontal AOA λ and the vertical AOA φ are measured by observing the arriving angles of the signal coming from the mobile (Fig. 1). With n_φ and n_λ the measurement noises associated with λ and φ, they can be obtained by:

$$\begin{aligned} \lambda &= \tan^{-1}\left(\frac{y}{x}\right) + n_\lambda, \\ \varphi &= \tan^{-1}\left(\frac{z}{\sqrt{x^2+y^2}}\right) + n_\varphi \end{aligned} \tag{1}$$

Pedestrian navigation is applied in a local reference frame (LRF), usually related to the building's infrastructure. (E, N, Z) and (x, y, z) are respectively the coordinates of M in the LRF and in the BSRF. Therefore the AOA of interest are expressed in the LRF thanks to the rotation matrix R.

$$\begin{aligned} \mathbf{X}^T = \begin{bmatrix} E & N & Z \end{bmatrix}^T &= \mathbf{R} \begin{bmatrix} x & y & z \end{bmatrix}^T \\ &= \begin{bmatrix} \cos(\alpha)\cos(\beta) & -\sin(\alpha) & \cos(\alpha)\sin(\beta) \\ \sin(\alpha)\cos(\beta) & \cos(\beta) & \sin(\alpha)\sin(\beta) \\ -\sin(\beta) & 0 & \cos(\beta) \end{bmatrix} \begin{bmatrix} x \\ y \\ z \end{bmatrix} \end{aligned} \tag{2}$$

where the pan angle α and the tilt angle β describe the orientation of the BS in the LRF. Practically, the horizontal

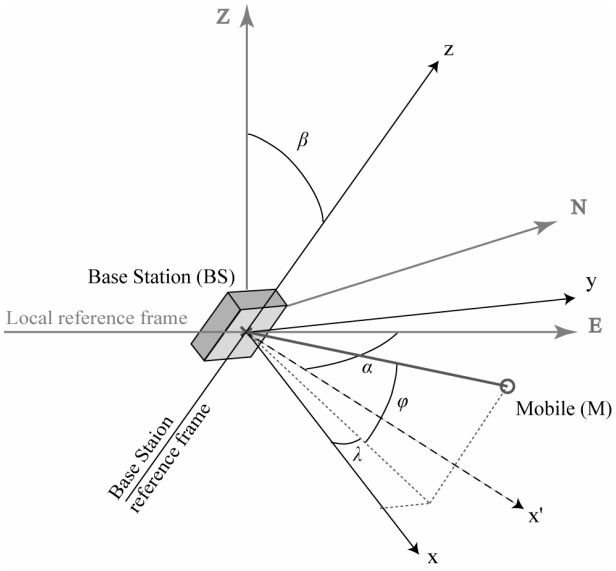

Fig. 1. AOA Measurement

orientation of the BS is parallel to the ground and the associated angle is neglected. In the LRF, (1) becomes:

$$\lambda = \tan^{-1}\left(\frac{N-N_i}{E-E_i}\right) - \alpha_i + n_\lambda \tag{3}$$

$$\varphi = \tan^{-1}\left(\frac{Z-Z_i}{\sqrt{(E-E_i)^2+(N-N_i)^2}}\right) - \beta_i + n_\varphi \tag{4}$$

It is noted that (E_i, N_i, Z_i) corresponds to the coordinates of the BS_i.

The geometrical location of the mobile M described by one AOA is given by:

$$\mathbf{M} \in \mathbb{R}^3 : \begin{cases} \mathbf{M} = \mathbf{BS} + k\,\mathbf{s} \\ \mathbf{s} = \begin{bmatrix} \cos(\varphi+\beta)\cos(\lambda+\alpha) \\ \cos(\varphi+\beta)\sin(\lambda+\alpha) \\ \sin(\varphi+\beta) \end{bmatrix} \\ \forall k \in \mathbb{R} \end{cases} \tag{5}$$

While **s** is defined as a unit vector of the line (BS, M), k corresponds to the range between BS and M.

B. Modelling of time difference of arrival

To estimate a TDOA, we first measure the times of arrival (TOA) of a given signal on two different receivers and we compute their difference. TDOA measurement Δt_{ij} between the *ith* and *jth* BS is computed from:

$$\Delta t_{i,j} = \frac{1}{c}\left(d(M, BS_i) - d(M, BS_j)\right) + n_{\Delta t_{ij}} \tag{6}$$

where

$$d(\mathrm{M},\mathrm{BS}_k) = \sqrt{(\mathrm{E}_k - \mathrm{E})^2 + (\mathrm{N}_k - \mathrm{N})^2 + (\mathrm{Z}_k - \mathrm{Z})^2},$$
$$k \in \{i, j\}$$

c is the speed of light. The measurement is contaminated with noises from both TOA measurements on both BS. It is denoted $n_{\Delta ij}$ in (7).

The fundamental theorem in conventional hyperbolic range difference location systems is: "The difference in range to two known stations provides a hyperbolic line of positions". In R^3, the geometrical location of M described by one TDOA corresponds then to a hyperboloid whose BS are the foci. Its parametric equation $f(u,v)$ can be written as:

$$\mathbf{X} = a\cosh(u)\,\boldsymbol{nx} + b\sinh(u)\cos(v)\,\boldsymbol{ny} + b\sinh(u)\sin(v)\,\boldsymbol{nz} + \boldsymbol{sm} \quad (7)$$

with $u \in [-\infty, +\infty]$ and $v \in [0, \pi]$.

a and b are the coefficients of the hyperboloid. ***sm*** corresponds to the origin of the hyperbolic reference frame whose normalized axis are defined by the mutually perpendicular vectors (***nx***, ***ny***, ***nz***). All variables are represented on Fig. 2.

The associated Cartesian equation can be expressed as:

$$1 = \frac{x^2}{a^2} - \frac{y^2}{b^2} - \frac{z^2}{b^2} \quad (8)$$

C. Location estimation based on two AOA

Two lines corresponding to two AOA intersect to a single point if the measurements are line of sight (LOS) and noiseless. Otherwise only their projections onto a plane intersect. If they don't intersect at a single point, they can be connected by a line segment. The midpoint of the shortest line segment is unique and is considered to be their intersection in 3D.

The shortest line segment [P_1, P_2] between two AOA lines, defined by their base stations (BS_1, BS_2) and their direction vectors ($\mathbf{s_1}$, $\mathbf{s_2}$), is perpendicular to the two lines.

$$\begin{cases} \overrightarrow{\mathrm{P_1P_2}} \cdot \mathbf{s_1} = 0 \\ \overrightarrow{\mathrm{P_1P_2}} \cdot \mathbf{s_2} = 0 \end{cases}, \quad (9)$$
$$\mathbf{P_i} = \mathbf{BS_i} + k_i\,\mathbf{s_i}, \quad i \in \{1,2\}$$

Expanding (6), it is possible to compute the distances k_1 and k_2 as follows:

$$\mathrm{k_1} = \frac{(\mathbf{BS_1} - \mathbf{BS_2})^{\mathrm{T}} \left((\mathbf{s_2}^{\mathrm{T}}\mathbf{s_1})\mathbf{s_2} - \|\mathbf{s_2}\|^2 \mathbf{s_1} \right)}{\|\mathbf{s_2}\|^2 \|\mathbf{s_1}\|^2 - (\mathbf{s_2}^{\mathrm{T}}\mathbf{s_1})^2},$$

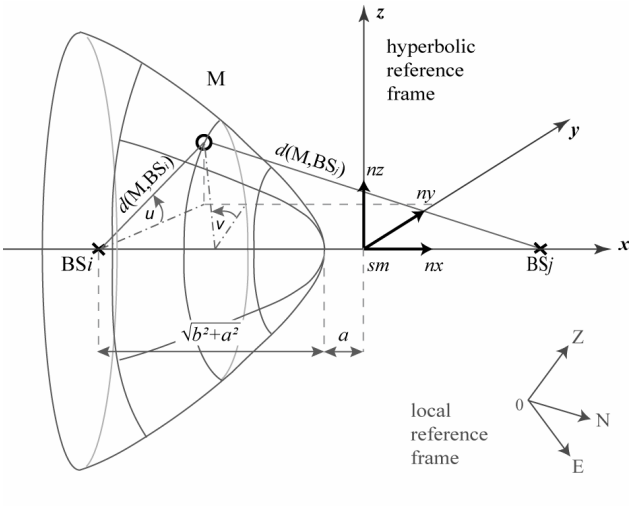

Fig. 2. TDOA Measurement

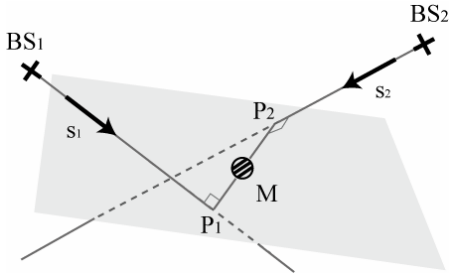

Fig. 3. Intersection of two AOA

$$\mathrm{k_2} = \frac{(\mathbf{BS_1} - \mathbf{BS_2})^{\mathrm{T}} \left(\|\mathbf{s_1}\|^2 \mathbf{s_2} - (\mathbf{s_2}^{\mathrm{T}}\mathbf{s_1})\mathbf{s_1} \right)}{\|\mathbf{s_2}\|^2 \|\mathbf{s_1}\|^2 - (\mathbf{s_2}^{\mathrm{T}}\mathbf{s_1})^2} \quad (10)$$

The coordinates of M can be associated with the middle of the line segment and are obtained by:

$$\mathbf{M} = \frac{1}{2}(\mathbf{BS_1} - \mathbf{BS_2} + \mathrm{k_1}\mathbf{s_1} - \mathrm{k_2}\mathbf{s_2}) \quad (11)$$

D. Location estimation based on one AOA and one TDOA

A hyperboloid and a 3D line intersect either on a single point (Fig. 4b.), either on two different points (Fig. 4a.) or has no solution. Equation (7) that describes the location of M based on one TDOA can be expressed in a vector form:

$$\mathbf{X} = \begin{bmatrix} \boldsymbol{nx} & \boldsymbol{ny} & \boldsymbol{nz} \end{bmatrix} \begin{bmatrix} a\cosh(u) \\ b\sinh(u)\cos(v) \\ b\sinh(u)\sin(v) \end{bmatrix} + \boldsymbol{sm} = \mathbf{R} \cdot \mathbf{x} + \boldsymbol{sm} \quad (12)$$

Combining (5) and (11), we obtain the following equation:

$$\mathbf{x} = \mathbf{R}^{\mathrm{T}}(k\,\mathbf{s} + \mathbf{BS} - \boldsymbol{sm}) \tag{13}$$

Equation (13) combined with (8) becomes a quadratic polynomial in k.

$$0 = \mathrm{A}\,k^2 + \mathrm{B}\,k + \mathrm{C} \tag{14}$$

where

$$\mathrm{A} = b^2(\boldsymbol{nx}^{\mathrm{T}}\mathbf{s})^2 - a^2\left((\boldsymbol{ny}^{\mathrm{T}}\mathbf{s})^2 + (\boldsymbol{nz}^{\mathrm{T}}\mathbf{s})^2\right)$$

$$\mathrm{B} = 2\left(b^2(\boldsymbol{nx}^{\mathrm{T}}\mathbf{s})(\boldsymbol{nx}^{\mathrm{T}}\mathbf{Q}) - a^2\left((\boldsymbol{ny}^{\mathrm{T}}\mathbf{s})(\boldsymbol{ny}^{\mathrm{T}}\mathbf{Q}) + (\boldsymbol{nz}^{\mathrm{T}}\mathbf{s})(\boldsymbol{nz}^{\mathrm{T}}\mathbf{Q})\right)\right),$$

$$\mathrm{C} = b^2(\boldsymbol{nx}^{\mathrm{T}}\mathbf{Q})^2 - a^2\left((\boldsymbol{ny}^{\mathrm{T}}\mathbf{s})^2 + (\boldsymbol{nz}^{\mathrm{T}}\mathbf{s})^2\right) - a^2b^2,$$

$$\mathrm{Q} = \mathbf{BS} - \boldsymbol{sm}$$

A classical analysis of the discriminant Δ of (14) provides two types of solutions (Fig. 4). The intersections of the AOA and the TDOA measurement are then computed based on the known BS coordinates and the pseudo range k.

E. 3D Hyperbolic intersection based on two TDOA

A number of solutions that address the problem of geolocation based on TDOA have been presented in the literature. Reference [6] was the first to provide a 3D closed form solution that doesn't depend on range data. This method offers good performances with the assumption that the measurements are noise free. However the closed form solution requires four independent BS to process a solution. Furthermore if the time synchronisation between M and the BS is kept as unknown, the solution needs TDOA recorded on five BS at the same time, which is hardly achievable in realistic indoor environment. Taylor series expansion methods were used in [7, 8] to estimate the mobile location from TDOA data. These techniques require iterative processes and may suffer from the convergence problem due to an incorrect initial guess of the mobile position. An alternative to 2D hyperbolic position fix was proposed by [9] with a two steps Least Squares (LS) approach that is an approximate realization of the Maximum Likelihood (ML) Estimator. This scheme is a non iterative process. Good performances are obtained with LOS measurements.

The first step of the last scheme is adapted to compute the geometrical intersections of two TDOA in R^3. The distance between M and the kth BS is given by:

$$\begin{aligned} d(\mathrm{M},\mathrm{BS}_k)^2 &= (\mathrm{E}_k - \mathrm{E})^2 + (\mathrm{N}_k - \mathrm{N})^2 + (\mathrm{Z}_k - \mathrm{Z})^2 \\ &= \mathrm{K}_k - 2\mathrm{E}_k\mathrm{E} - 2\mathrm{N}_k\mathrm{N} - 2\mathrm{Z}_k\mathrm{Z} + \mathrm{E}^2 + \mathrm{N}^2 + \mathrm{Z}^2 \end{aligned} \tag{15}$$

with $\mathrm{K}_k = \mathrm{E}_k^2 + \mathrm{N}_k^2 + \mathrm{Z}_k^2$

With measurements that are free of noise and $j=1$, (6) can be rewritten as follows.

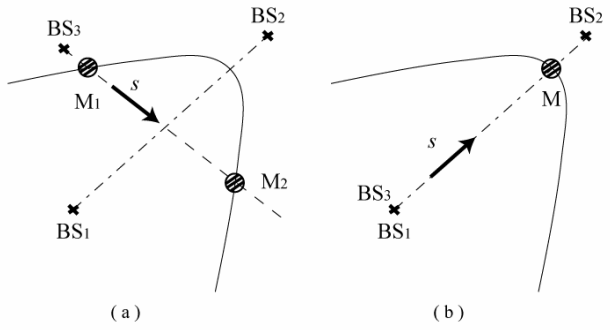

Fig. 4. Intersection of one AOA and one TDOA

$$d(\mathrm{M},\mathrm{BS}_i)^2 = \left(c\Delta\mathrm{t}_{i,1} + d(\mathrm{M},\mathrm{BS}_1)\right)^2 \tag{16}$$

Subtracting $d(\mathrm{M},\mathrm{BS}_1)^2$ from (16), it is possible to transform (15) in a set of linearized equations in (E, N, Z, $d(\mathrm{M},\mathrm{BS}_1)$).

$$\begin{aligned} &\mathrm{E}(\mathrm{E}_i - \mathrm{E}_1) + \mathrm{N}(\mathrm{N}_i - \mathrm{N}_1) + \mathrm{Z}(\mathrm{Z}_i - \mathrm{Z}_1) + c\Delta\mathrm{t}_{i,1}d(\mathrm{M},\mathrm{BS}_1) \\ &= \frac{1}{2}\left(\mathrm{K}_i - \mathrm{K}_1 - \left(c\Delta\mathrm{t}_{i,1}\right)^2\right) \end{aligned} \tag{17}$$

When times of flight are available at the same instant on four different BS, the location of M can be computed as a function of $d(\mathrm{M},\mathrm{BS}_1)$ based on (17). Substitution of these coordinates in (15) produces a quadratic polynomial in $d(\mathrm{M},\mathrm{BS}_1)$. The location of M is estimated injecting the positive root back of the quadratic form in (17).

Considering the challenges of real indoor environments and the limitations of UWB propagation due to the human body, a more realistic approach using only three different BS is presented. As the height of a pedestrian changes rarely indoors, the last one is considered as a constant Z_0 between two epochs. Therefore the vector form of (17) can be expressed as:

$$\begin{aligned} \begin{bmatrix} \mathrm{E} \\ \mathrm{N} \end{bmatrix} = \begin{bmatrix} \mathrm{E}_2 - \mathrm{E}_1 & \mathrm{N}_2 - \mathrm{N}_1 \\ \mathrm{E}_3 - \mathrm{E}_1 & \mathrm{N}_3 - \mathrm{N}_1 \end{bmatrix}^{-1} \times \Bigg\{ \frac{1}{2}\begin{bmatrix} \mathrm{K}_2 - \mathrm{K}_1 - \left(c\Delta\mathrm{t}_{2,1}\right)^2 \\ \mathrm{K}_3 - \mathrm{K}_1 - \left(c\Delta\mathrm{t}_{3,1}\right)^2 \end{bmatrix} \cdots \\ \cdots - \mathrm{Z}_0\begin{bmatrix} \mathrm{Z}_2 - \mathrm{Z}_1 \\ \mathrm{Z}_3 - \mathrm{Z}_1 \end{bmatrix} - c\,d\left(\mathrm{M},\mathrm{BS}_1\right)\begin{bmatrix} \Delta\mathrm{t}_{2,1} \\ \Delta\mathrm{t}_{3,1} \end{bmatrix} \Bigg\} \end{aligned} \tag{18}$$

In the final fusion filter, the height is fixed from the user state at the previous instant.

Equation (18) expresses the coordinates E and N as a function of $d(\mathrm{M},\mathrm{BS}_1)$ only if $(\mathrm{E}_2\text{-}\mathrm{E}_1)(\mathrm{N}_3\text{-}\mathrm{N}_1)$ is not equal to $(\mathrm{E}_3\text{-}\mathrm{E}_1)(\mathrm{N}_2\text{-}\mathrm{N}_1)$. This condition translates the non colinearity of the three BS involved. The geometry formed by the BS impacts the accuracy of the location estimation technique. The best results are obtained when the BS are placed on the corners of the volume considered [10], for example the room's corners. These corners represent the edges of the

corresponding tetrahedron. Indoors, BS equip mainly corridors and rooms. While walking inside buildings, the probability to record time metrics on aligned BS is pretty low.

For simplicity, we set $E_{ij}=E_i-E_j$, $N_{ij}=N_i-N_j$, $Z_{ij}=Z_i-Z_j$ and $K_{ij}=K_i-K_j$. (18) is expanded to express (E, N) as a set of linear equations.

$$\begin{cases} E = g_E + h_E\, d(M, BS_1) \\ N = g_N + h_N\, d(M, BS_1) \end{cases} \tag{19}$$

where

$$q = E_{21}N_{31} - E_{31}N_{21}$$

$$g_E = \frac{1}{2q}\left(N_{31}K_{21} - N_{21}K_{31} + c^2(N_{21}\Delta t_{3,1}^2 - N_{31}\Delta t_{2,1}^2)\ldots \right.$$
$$\left. \ldots + 2Z_0(N_{21}Z_{31} - N_{31}Z_{21})\right),$$

$$h_E = \frac{c}{q}\left(N_{21}\Delta t_{3,1} - N_{31}\Delta t_{2,1}\right),$$

$$g_N = \frac{1}{2q}\left(E_{21}K_{31} - E_{31}K_{21} + c^2(E_{31}\Delta t_{2,1}^2 - E_{21}\Delta t_{3,1}^2)\ldots \right.$$
$$\left. \ldots + 2Z_0(E_{31}Z_{21} - E_{21}Z_{31})\right),$$

$$h_N = \frac{c}{q}\left(E_{31}\Delta t_{2,1} - E_{21}\Delta t_{3,1}\right)$$

Introducing (19) in (15), we obtain the following quadratic polynomial in $d(M,BS_1)$:

$$2\left(h_E(E_1 - g_E) + h_N(N_1 - g_N)\right)d(M, BS_1) + (1 - h_E^2 - h_N^2)d(M, BS_1)^2$$
$$= K_1 - 2\left(E_1 g_E + N_1 g_N + Z_1 Z_0\right) + g_E^2 + g_N^2 + Z_o^2 \tag{20}$$

Substitution of the positive root back into (19) produces the solution that is the coordinates of the intersection of two TDOA with a fixed known height.

III. Walking Features Based on MEMS Data

MEMS result from the integration of mechanical and electrostatic elements on a common substrate. Accelerometers, gyroscopes and magnetometers are the main sensors based on this technology. They record inertial data used for pedestrian navigation in a dead reckoning mode. Compact and relatively cheap, MEMS sensors allow the quantification of a user's displacement using integration techniques or pattern recognition [11-13]. These techniques often rely on estimation models or statistical data to track the step length or the horizontal speed of the user in real time.

The inertial measurement unit (IMU XSens [14], Fig. 5) is composed of a triad of orthogonal accelerometers, a triad of orthogonal gyroscopes and a triad of orthogonal magnetometers. This module is carried by the user on the trunk, combined with the UWB tag. The walking features of the pedestrian are described by biomechanical information issued from the MEMS records [15].

Fig. 5. XSens inertial measurement unit

Accelerometers data detect steps. A process, consisting of a sliding window associated with a threshold, analyses the vertical accelerations to identify the steps. Gyroscopes and magnetometers are used to estimate the pedestrian's heading.

Although MEMS sensors provide regular and independent data, the latter are affected by errors typical of these sensors which can disturb the estimation of the footpath. Experience shows that the main source of error is induced by the azimuth component. Filters [16, 17] have difficulties to compensate the measurements of the Earth's magnetic field disturbed by magnetic perturbations especially under high dynamic, for example during walking, or in unpredictable magnetically perturbed environments. If no additional absolute measurement is available, the MEMS-based trajectory's error might grow rapidly in time. To cope with this difficulty, MEMS are often hybridised with other positioning technologies. In these hybridisation schemes, their records compensate the lack of regularity of absolute measurement systems [18].

IV. The Proposed Pedestrian Navigation Algorithm

In this section, the proposed pedestrian navigation algorithm based on MEMS and UWB observations is detailed. The Extended Kalman Filter (EKF) [19] that drives the fusion process is first depicted. The robust regression method complementing the filter to mitigate the Non Line of Sight (NLOS) UWB propagation is then explained. A selection method of LOS signals and the impact of the human body on the transmission of UWB radio signals are also presented.

A. System model of the fusion filter

The step detection is an event driven information based on MEMS observations that follows the walking rhythm. UWB pulses are emitted at a regular rate, but the availability of the associated metrics depends on the environment configuration and the human body interaction. Therefore the mechanisation part of the filter is automatic. The state vector is:

$$\mathbf{x} = \left[E \quad N \quad Z \quad v_z \quad f_{step} \quad l_{step} \quad \theta_{MEMS} \quad \delta\theta_{MEMS}\right]^T \tag{21}$$

where

E, N, Z are the East, North and height components of the pedestrian position

v_z is the vertical speed
f_{step} is the frequency of the pedestrian steps
l_{step} is the pedestrian step's length
θ_{MEMS} is the MEMS based walking heading
$\delta\theta_{MEMS}$ is the MEMS based heading perturbation

The process model consists of a classical dead reckoning mechanisation:

$$\begin{aligned} \dot{E} &= f_{step} \cdot l_{step} \cdot \sin(\theta_{MEMS} + \delta\theta_{MEMS}) \\ \dot{N} &= f_{step} \cdot l_{step} \cdot \cos(\theta_{MEMS} + \delta\theta_{MEMS}) \\ \dot{Z} &= v_z \end{aligned} \quad (22)$$

f_{step} is associated with a white noise stochastic model and is updated by the step detection process. The user's horizontal speed is computed by multiplying f_{step} with the step length l_{step}. MEMS-based headings are affected by a bias that varies strongly with time. These variations are mainly due to magnetic perturbations. Therefore the estimation of the associated deviation $\delta\theta_{MEMS}$ is essential to achieve good performance.

B. *Measurement models of the fusion filter*

MEMS observations are directly related to the state variables f_{step} and θ_{MEMS} leading to linear measurement models. UWB observations consist in AOA and TDOA metrics. Equations (3) and (4) detail the AOA measurements models while (6) describe the TDOA measurement model.

C. *Robust regression method: RANSAC*

Contrary to MEMS data, the availability of UWB measurements is particularly irregular in time. In fact, the geometrical configuration drawn by the mobile and the base stations affects the UWB propagation. Geolocation techniques often suppose that the received signals propagate through LOS path, but a large part of the observations consists in NLOS paths introducing errors in range measurements and leading to erroneous location estimation. Kalman filtering assumes that the noise terms are Gaussian, but NLOS measurements don't fulfil this hypothesis. The associated error corresponds to an excessive travelling distance compared with the direct path. It leads the EKF to diverge, as it can not approximate the true distribution. Therefore the need to identify reflected signals before introducing them in the fusion process is crucial.

Several algorithms pursuing that goal have been presented in the literature. Algorithms [20, 21] require knowledge of NLOS error statistics or time history of UWB measurements to reconstruct the LOS path. They work well when the mobile is moving and the environment influence is known. Iterative algorithms [7] based on Taylor Series address also the NLOS problem but they often rely on an initial value which reliability affects the convergence. Geolocation technique based on adaptive autoregressive models [22] has been presented to eliminate the NLOS measurements. This two step algorithm relies on a robust filter cleaner which choice of the weight function is critical. A new robust method based on the Random Sample Consensus (RANSAC) paradigm [23] is proposed to mitigate the effect of NLOS propagation in the case of pedestrian navigation.

Commonly used in computer vision, RANSAC can interpret smoothing data that contain a significant percentage of gross error. It chooses a subset of the data by random sampling and estimates a model for each subset. The number of points in the subset is equal to the number of unknown model parameters, yielding closed form solutions. The robustness of RANSAC is contingent on the existence of at least one subset of data carrying the correct model.

The walking features of a person, such as the speed v and the heading θ, are constrained by physical parameters. Experiments have shown that v varies between 0 and 2 to 3 metre per second. Furthermore over a very short period, the footpath can be considered as a straight line and the heading as a constant. Consequently the proposed RANSAC process considers a walk model (23) which parameters are v and θ to fit the UWB positions resulting from the geometry based algorithms described in section 2.

$$f(v,\theta) = v \cdot \tan(\theta) = \frac{\sqrt{\Delta E^2 + \Delta N^2}}{\Delta t} \tan\left(\frac{\Delta E}{\Delta N}\right) \quad (23)$$

The random sampling deals with a 0.5 second sliding window. UWB pulses are emitted at 5 Hz but the accuracy of UWB LOS position estimation is about 20 centimetres. Working with a half second window insures that the speed error tolerance is below the error induced by the UWB geometry based algorithms in the case of LOS signals. A major interest of this robust selection consists in observing differential UWB metrics instead of epoch to epoch radio signals. As a consequence walking patterns that might be reflected but which are consistent over a short time period will also be considered. This increases the amount of data used in the fusion algorithm but is not appropriate to select AOA and TDOA metrics issued from LOS paths useful for the update of the state.

D. *Selection method of LOS metrics*

The selection of LOS radio signals is made by comparing the predicted state with the UWB positions computed thanks to the geometry based algorithms. The standard deviations derived from the predicted covariance matrix according to a variance propagation scheme are used to define thresholds. The last are used to assess the final choice of UWB positions and thus the corresponding UWB metrics.

E. *Impact of the human body on radio signals propagation*

Finally the limitations due to the human body absorption of UWB radio signals is considered. Many experiments have been conducted to assess whether the human body represents an obstacle for UWB electromagnetic waves propagation or not. [24, 25] demonstrate that the human body absorbs a large part of UWB signals. In our experiment, the UWB tag is carried on the trunk, suspended around the neck. Consequently UWB metrics involving BS located behind the

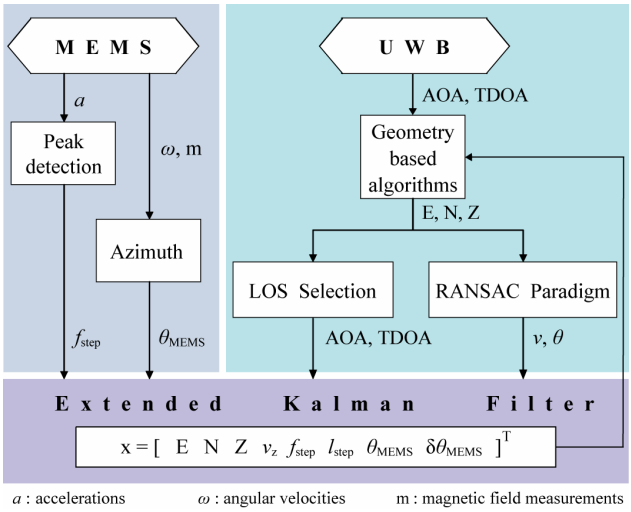

Fig. 6. MEMS/UWB data fusion architecture

pedestrian result only from NLOS signals. A selection method [19] compares the EKF predicted heading with the angle between the BS and the state position to eliminate the corresponding reflected radio signals.

Fig. 6 summarises the proposed MEMS/UWB data fusion scheme for pedestrian navigation.

V. Performance Evaluation of the Fusion Algorithm

Experimental tests were conducted in a classroom of EPFL campus, where the UWB localisation system from Ubisense [26] is installed. During these tests, a pedestrian equipped with the IMU module and an UWB tag (Fig.7) is walking following clearly defined footpaths.

The reference trajectories are marked with waypoints on the ground, whose coordinates are known. MEMS and UWB data are stored on a computer. Hybrid routes are computed with the fusion filter. To evaluate the proposed solution, the fusion filter is compared with the pure inertial localisation technique. The pedestrian's reference trajectories are created by storing each instant the person walks on a waypoint. The distance to each waypoint is computed and associated RMS values are estimated.

$$\text{error} = \sqrt{(E - E_{ref})^2 + (N - N_{ref})^2} \qquad (24)$$

In Fig. 8 and Fig. 9, we can observe the experimental test results plotted together with the classroom map in the background. Two different scenarii were repeated several times. During the second scenario, the pedestrian sits on a chair at the position marked with the sign "stop" visible on Fig. 9. It is important to notice that all walls of the experimental room are made of steel, which increases the effect of multipath and the percentage of NLOS measurements in the UWB dataset.

In all runs, the hybrid navigation solution performs better than the pure inertial solution depicted with a dashed black

Fig. 7. Ubisense UWB tag

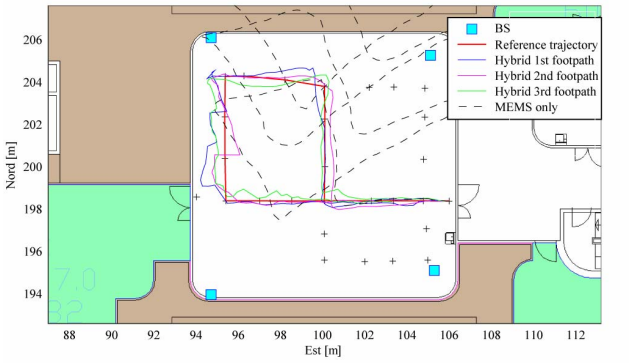

Fig. 8. Footpaths for the 1st scenario.

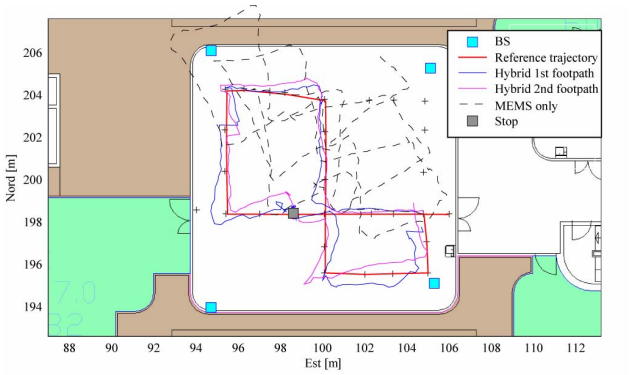

Fig. 9. Footpaths for the 2nd scenario.

line. This can easily be observed by the fact that the fusion filter keeps all routes in the 145 square metres classroom whereas the MEMS based footpaths exit the room.

Jumps in the position along some straight footpaths can be observed. The pedestrian is sometimes located in unfavourable geometrical configurations causing a lack of measurements or NLOS signals only. In this case, the navigation solution relies only on inertial data and the route drifts until new UWB metrics are available.

Whereas the hybrid positions remain close to the reference trajectories, maximum error between the true and hybrid positions generally happens while the pedestrian is turning. The smoothing effect of the EKF reduces its capacity to follow the pedestrian dynamics when rapid changes in speed and heading occur.

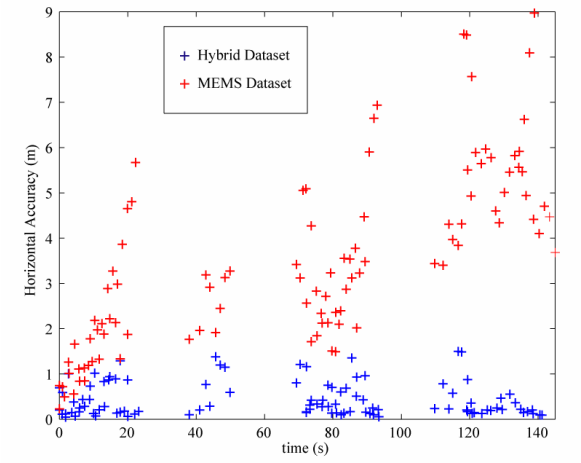

Fig. 10. Comparison of the horizontal accuracy obtained with the hybrid and dead reckoning navigation solutions

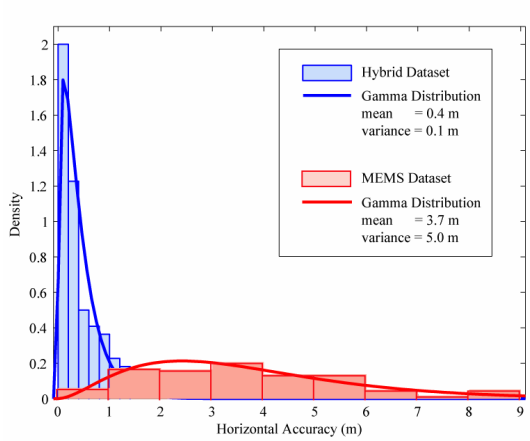

Fig. 11. Probability density functions of the planimetric errors computed at each waypoint

Fig. 10 depicts the evolution in time of the horizontal error between the reference trajectory and the computed positions at each waypoint, in red for the hybrid solution and in blue for the MEMS-based positions. As expected the pure inertial error grows with time, whereas the fusion filter generally keeps the error below 1 metre. The analysis of the probability density functions (PDF) depicted in Fig. 11 confirms this phenomenon.

Computed as the quadratic sum of two independent Gaussian random variables, the horizontal error follows gamma PDF drawn in blue for the hybrid dataset and in red for the MEMS based dataset.

The good performance of the fusion filter is confirmed by the average of the position errors that remains below 1 metre with a 0.1 metre variance. The histogram of the MEMS based position errors has a flattened feature with 3.7 metre average. It is more scattered than the hybrid one. The 5 metre variance reflects the wide dispersion of the errors around the mean value.

The height component of the fusion filter relies only on the UWB radio signals. The MEMS based step frequency and heading give information only for horizontal displacements. Nevertheless, the use of a first order Gauss Markov model for vertical speed modelling produces good performance. The vertical average accuracy is equal to 0.2 metre even with the height variations when the pedestrian is sitting.

VI. CONLUSION

This paper describes a novel optimal data fusion filter based on UWB radio signals and MEMS data especially designed for pedestrian navigation in R^3. First experimental results are promising. Hybridised trajectories present improved performances in terms of position precision and reliability compared with the pure inertial navigation solution.

New procedures, that complement the EKF, play a major role in this improvement. The geometry based position estimation algorithms combined with the history of the EKF state of the user result in a better selection of the LOS. The use of a RANSAC paradigm customised to the human walking motion increases the amount of available data for the coupling filter. Both specific developments mitigate the impact of NLOS. The efficiency of the proposed solution generally enabled us to localize the pedestrian within a metre, which addresses the user's needs for indoor localisation.

Although these results are based on a limited dataset, we believe that achieving good performances in the challenging environment of the experimental room demonstrates the validity of the proposed fusion filter to provide realistic solution for indoor pedestrian navigation. To complete this study, additional tests performed in larger environments should be considered. These tests would help, for example, to evaluate the impact of the stochastic behaviour of the pedestrian on the navigation performances. Considering the diversity of the methods involved in the proposed solution, guiding a pedestrian indoors requires a wide range of skills, and some taste to combine them.

REFERENCES

[1] "FCC Docket No. 94-102. Revision of the Commission's Rules to Ensure Compatibility with Enhanced 911 Emergency Calling Systems," Federal Communication Commission RM. 8143, July 1996.

[2] EC, "Directive of the European Parlament and of the council on universal service and users' rights relating to electronic communications networks and services," Commission of the European Communities, 2000.

[3] A. H. Sayed, A. Tarighat, and N. Khajehnouri, "Network-based wireless location," *IEEE Signal Processing Magazine*, vol. 22, pp. 24-40, 2005.

[4] V. Renaudin, O. Yalak, P. Tomé, and B. Merminod, "Indoor Navigation of Emergency Agents," *European Journal of Navigation*, vol. 5, pp. 36-45, 2007.

[5] N. El-Scheimy and X. Niu, "The Promise of MEMS to the Navigation Community," *Inside GNSS*, vol. 2, pp. 46-56, 2007.

[6] E. G. Bakhoum, "Closed-form solution of hyperbolic geolocation equations," *IEEE Transactions on Aerospace and Electronic Systems*, vol. 42, pp. 1396-1404, 2006.

[7] W. H. Foy, "Position-Location Solutions by Taylor-Series Estimation," *IEEE Transactions on Aerospace and Electronic Systems*, vol. 12, pp. 187-194, 1976.

[8] W. Wang, J. Y. Xiong, and Z. L. Zhu, "A new NLOS error mitigation algorithm in location estimation," *IEEE Transactions on Vehicular Technology*, vol. 54, pp. 2048-2053, 2005.
[9] Y. T. Chan and K. C. Ho, "A Simple and Efficient Estimator for Hyperbolic Location," *IEEE Transactions on Signal Processing*, vol. 42, pp. 1905-1915, 1994.
[10] Z. Ebrahimian and R. A. Scholtz, "Receiver sites for accurate indoor position location systems," presented at IEEE/ACES International Conference on Wireless Communications and Applied Computational Electromagnetics, Honolulu, HI, 2005.
[11] Q. Ladetto and B. Merminod, "In step with INS - Navigation for Blind, Tracking Emergency Crews," *GPS World*, vol. 13, pp. 30-38, 2002.
[12] O. A. Mezentsev, "Sensor aiding of HSGPS pedestrian navigation," doctoral dissertation, Dept. Geomatic Engineering, University of Calgary, 2005.
[13] G. Retscher and M. Thienelt, "NAVIO – A Navigation and Guidance Service for Pedestrians," presented at The International Symposium on GNSS/GPS, Sydney, 2004.
[14] www.xsens.com
[15] K. Aminian and B. Najafi, "Capturing human motion using body-fixed sensors: outdoor measurement and clinical applications," *Computer animation and virtual worlds*, vol. 15, pp. 79–94, 2004.
[16] D. Roetenberg, H. J. Luinge, C. T. M. Baten, and P. H. Veltink, "Compensation of magnetic disturbances improves inertial and magnetic sensing of human body segment orientation," *IEEE Transactions on Neural Systems and Rehabilitation Engineering*, vol. 13, pp. 395-405, 2005.
[17] A. M. Sabatini, "Quaternion-based extended Kalman filter for determining orientation by inertial and magnetic sensing," *IEEE Transactions on Biomedical Engineering*, vol. 53, pp. 1346-1356, 2006.
[18] V. Renaudin, O. Yalak, and P. Tomé, "Hybridization of MEMS and Assisted GPS for Pedestrian Navigation," *Inside GNSS*, vol. January/February, pp. 34-42, 2007.
[19] S. Pittet, V. Renaudin, B. Merminod, and M. Kasser, "UWB and MEMS based indoor navigation," *Journal of Navigation*, in press.
[20] M. I. Wylie and J. Holtzman, "The non-line-of-sight problem in mobile location estimation," presented at 5th IEEE International Conference on Universal Personal Communications, Cambridge, MA, USA, 1996.
[21] D. B. Jourdan, J. J. Deyst, M. Z. Win, and N. Roy, "Monte Carlo Localization in Dense Multipath Environments Using UWB Ranging," presented at IEEE International Conference on Ultra-Wideband, Zürich, Switzerland, 2005.
[22] Z. Jie and Z. Shufang, "Adaptive AR model based robust mobile location estimation approach in NLOS environment," presented at IEEE 59thVehicular Technology Conference, 2004.
[23] M. A. Fischler and R. C. Bolles, "Random Sample Consensus: A Paradigm for Model Fitting with Applications to Image Analysis and Automated Cartography," *Graphics and Image Processing*, vol. 24, pp. 381-395, 1981.
[24] Y. P. Zhang, L. Bin, and C. Qi, "Characterization of on-human-body UWB radio propagation channel," *Microwave and Optical Technology Letters*, vol. 49, pp. 1365-1371, 2007.
[25] T. B. Welch, R. L. Musselman, B. A. Emessiene, P. D. Gift, D. K. Choudhury, D. N. Cassadine, and S. M. Yano, "The effects of the human body on UWB signal propagation in an indoor environment," *IEEE Journal on Selected Areas in Communications*, vol. 20, pp. 1778-1782, 2002.
[26] www.ubisense.net